RECONCILING DIATOM PRODUCTIVITY AND IRON FLUX IN THE SOUTHERN OCEAN

A Thesis
Presented to
The Academic Faculty

By

Jacqueline Grace Valett

In Partial Fulfillment
Of the Requirements for the Degree
Master of Science in Earth and Atmospheric Sciences

Georgia Institute of Technology

May, 2015

RECONCILING DIATOM PRODUCTIVITY AND IRON FLUX IN THE SOUTHERN OCEAN

Approved by:

Dr. Takamitsu Ito, Advisor
School of Earth and Atmospheric Sciences
Georgia Institute of Technology

Dr. Ellery Ingall
School of Earth and Atmospheric Sciences
Georgia Institute of Technology

Dr. Annalisa Bracco
School of Earth and Atmospheric Sciences
Georgia Institute of Technology

Date Approved: April 15, 2015

ACKNOWLEDGEMENTS

I wish to thank my advisor, Dr. Takamitsu Ito, for his guidance throughout the thesis process. I also wish to thank my committee members, Dr. Ellery Ingall and Dr. Annalisa Bracco, for their helpful comments and suggestions regarding this thesis.

TABLE OF CONTENTS

LIST OF TABLES

LIST OF FIGURES

SUMMARY

Iron plays an important role in the regulation of biological productivity and the carbon cycle of the Southern Ocean. Recently, synchrotron X-ray spectromicroscopy revealed that molar iron to silicon (Fe:Si) ratios in living diatom samples collected from surface waters and ice in the coastal Antarctic are significantly higher than reported dissolved Fe:Si ratios of Circumpolar Deep Water. Upwelling of Circumpolar Deep Water is a dominant source of iron and silicon to coastal Southern Ocean surface waters. Thus with higher Fe:Si ratios, diatom production preferentially depletes dissolved iron relative to silicon, potentially contributing to perennial iron limitation in this region. Combining diatom and water column dissolved iron and silicon datasets with a simple inverse box model we estimate the regional coupled iron and silicon budget. Upwelling of subsurface waters cannot supply enough iron to balance the loss due to diatom production, which indicates that the closed budget requires additional iron sources or additional methods of silicon removal. To evaluate the ecological and biogeochemical impacts of the high Fe:Si ratio, a three-dimensional ocean biogeochemistry and ecosystem model is used to simulate the sensitivity of ocean productivity and nutrient cycling to a wide range of Fe:Si ratios in modeled diatoms. The Fe:Si ratio of diatoms regulates the surface iron and macronutrient distribution in vast regions beyond the Southern Ocean. A globally higher Fe:Si ratio strongly decreases subpolar productivity and is partially compensated by the moderate increase in subtropical productivity. Our results indicate that the Fe:Si ratio of diatoms has a global impact controlling the distribution of both micro- and macro-nutrients and associated biological production.

CHAPTER 1

INTRODUCTION

The Southern Ocean (SO) plays a crucial role in global ocean circulation and biogeochemical cycling by transporting and transforming the nutrient and carbon chemistry of the major water masses (Speer et al. 2000, Sallée et al. 2013). The rich biological productivity of the SO has a direct influence on the regional carbon sink, partially offsetting the upwelling of excess carbon from the deep ocean. Iron availability is a key controller of phytoplankton growth within the SO as demonstrated by iron addition experiments (Martin et al. 1990, Boyd et al. 2012). Thus, understanding and characterizing iron cycling has become an increasingly important area of research.

Antarctic upwelling and its overturning circulation is a primary pathway for the input of nutrients that maintain productivity (Moore et al. 2001). The upper overturning cell of the SO consists of the upwelling of Upper Circumpolar Deep Water (Speer et al. 2000) and subsequent transformation into the northward flowing mode and intermediate waters (Figure 1, white arrows). This strong upwelling maintains a high level of macro-nutrients such as dissolved nitrate, phosphate, and silicate through the input of Circumpolar Deep Water. A percentage of global silicate (~50%) and phosphate (~15%) remain "trapped" in the SO (Holzer et al. 2014). Silicate and phosphate dissolve at mid-depth in upwelling deep water, which return the regenerated nutrients to the surface SO where they are utilized again and trapped in this continuous SO cycle (Holzer et al. 2014).

Due to low atmospheric dust input, iron enters the Southern Ocean mainly through the upwelling of deep waters. These upwelling water masses gain iron through

the remineralization of sinking organic matter and other subsurface sources such as hydrothermal vents, continental shelves, and icebergs (Boyd and Ellwood 2010, Tagliabue et al. 2010). The magnitudes of these iron sources appear to, at least partially, control biological productivity.

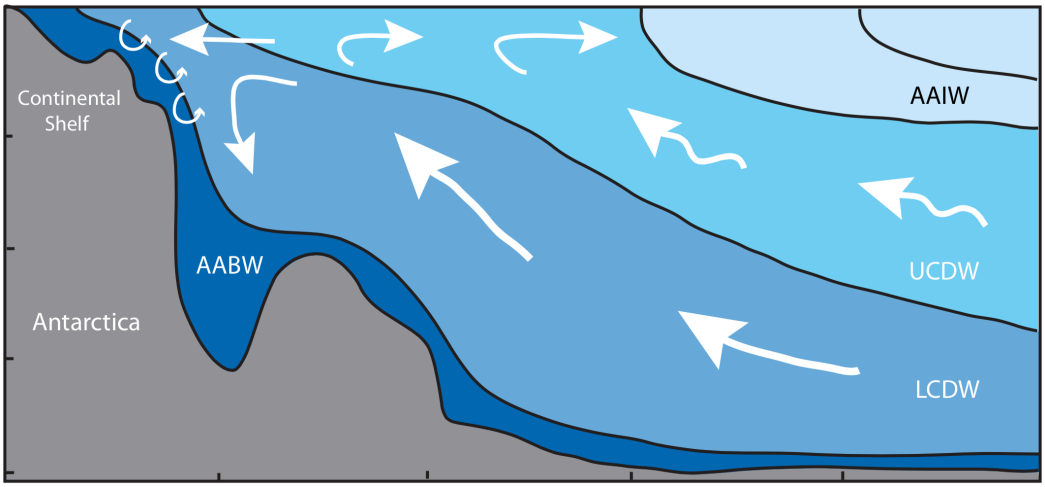

Figure 1. Overturning Circulation. Meridional overturning and water masses of the Southern Ocean reproduced from Speer et al., (2000). The white arrows indicate mass flux. AAIW = Antarctic Intermediate Water. UCDW = Upper Circumpolar Deep Water. LCDW = Lower Circumpolar Deep Water. AABW = Antarctic Bottom Water.

A unicellular algae, the diatom, predominates the phytoplankton community in the SO and has profound influences on regional biogeochemical cycles. Based on the spectral analysis of ocean color remote sensing, it is estimated that diatoms make up about 50% of the SO phytoplankton community during the productive summer months (Alvain et al. 2008). Diatom productivity may be limited primarily by available light and iron as well as other factors, and forms intense blooms near ocean fronts, edges of sea ice, and coastal Antarctica (Lancelot et al. 2000, Parekh et al. 2005). Each diatom is encased in a cell wall made of silica (hydrated silicon dioxide) called a frustule. Frustules can act

as a mineral ballast causing diatoms to sink more efficiently through the water column relative to organisms that do not contain mineral structures (Baines et al. 2010, Treguer and De La Rocha, 2013). Diatom productivity is a key factor in regulating the removal and export of nutrients from SO surface waters as a consequence of this efficient export mechanism.

A recent study proposed that the sedimentation of siliceous frustules with high iron to silicon (Fe:Si) ratios from SO surface waters provides an important removal mechanism for bioavailable iron (Ingall et al. 2013). Using synchrotron based analysis Ingall et al. (2013) showed that diatoms incorporate reduced organically-bound iron as a structural component deep within frustule silica. Even the most conservative estimate of frustal Fe:Si ratios measured after aggressive chemical treatments was still higher than that of the ambient water. Since frustles are dense and can rapidly sink downward in the water column, the structural iron incorporated into the frustle is protected from remineralization in the water column, providing an efficient removal pathway for the surface iron. Since the biological Fe:Si uptake ratio is higher than that of the ambient water, the production of every new diatom cell would shift the system towards iron depletion before the depletion of silicon (and other macro-nutrients). This issue will be addressed later in this thesis.

For the stoichiometry of macro-nutrients such as phosphate and nitrate, the N:P ratio of organic matter closely reflects that of the ambient water, indicative of the strong coupling between the stock of inorganic nutrients in the environment and biological sources and sinks (Redfield 1958). Observed micro-macro nutrient ratios appear to be more variable, potentially reflecting the variability of the stoichiometric ratio in organic

matter and/or the spatial decoupling of the environmental sources and sinks of these nutrients.

There are many aspects of iron cycling that are still unknown (Boyd et al. 2012). Given the low supply rate of iron, it has been a challenge to close the iron budget of the Southern Ocean (Tagliabue et al. 2012). In particular, factors controlling the speciation, complexation, and exchanges between dissolved and particulate forms of iron are all critically important to furthering research (Boyd and Ellwood 2010). In connection to the iron chemistry, sources of iron, especially within the Southern Ocean, have been hard to quantify due to sparse measurements and limited understanding in the changes undergone during transport in the ocean (Boyd et al. 2012). These difficulties, and the scarcity of sampling, are good reasons to use a model to look at the impacts of high iron uptake by diatoms. By modeling potential ocean and phytoplankton conditions we can begin to discover more about the mechanisms and interactions between diatoms and their nutrients without a complete set of observations.

Another obvious difficulty in understanding the high Fe:Si ratio of diatoms is that iron uptake by diatoms will make iron limitation more severe in the Southern Ocean, creating a potential negative feedback that regulates diatom growth. And yet, the evolutionary process has led the diatom to be the most dominant phytoplankton species in this region. This leads to a paradox of why diatoms, governed by the laws of natural selection and continuously under pressure from the challenges from other species, could be wasteful in consuming its own limiting nutrient. One way to reconcile this paradox could be to recognize that the ultimate cause of iron limitation in the Southern Ocean is the lack of major iron sources besides upwelling in the region, and phytoplankton species

compete against one another under this condition. Efficient iron removal by diatoms may prevent other species from utilizing iron such that apparent wasteful behavior may in fact be a good strategy to outcompete other phytoplankton species. In addition, intense mixing and wind-driven upwelling in this region may allow sinking diatoms and deep iron to mix back up into the surface waters during winter seasons, which may pre-condition the following spring/summer bloom.

The objectives of this thesis are (1) to quantify and constrain the circumpolar-scale cycling of iron and silicon using a simple box model of the Southern Ocean, and (2) to simulate diatom productivity and its role in regulating the cycling of micro- and macro-nutrients using a three-dimensional ocean circulation and biogeochemistry model. To achieve the first objective, we will use the existing datasets of dissolved inorganic iron and silicon and will reconcile these with the newly observed diatom Fe:Si ratios. This will provide constraints for the bulk elemental ratio averaged over the Southern Ocean. Secondly, we use a three-dimensional ocean ecosystem and biogeochemistry model as a tool to simulate the response of phytoplankton community and micro and macro-nutrient distributions given a range of iron to silicon ratios by performing a suite of sensitivity experiments. We conclude with a discussion of the implications of this thesis.

CHAPTER 2

METHODOLOGY

2.1 Observational Data

World Ocean Circulation Experiment (WOCE) cruises and a compilation of published iron measurements (Tagliabue et al. 2012) were used to evaluate the concentrations of dissolved iron and silicate in the major water masses in the SO. While tracer concentrations are not exactly uniform within each water mass, representative values can be estimated by averaging tracer concentrations within each density class. We follow (Sallée et al. 2013) for the density classifications of Subantarctic Mode Water (SAMW), Antarctic Intermediate Water (AAIW), Upper Circumpolar Deep Water (UCDW), North Atlantic Deep Water (NADW), and Antarctic Bottom Water (AABW) (Table 1). Representative concentrations of silicate were taken from WOCE data based on two hydrographic sections from the Atlantic (A16S and SR04), three from the Pacific (P15S, P17, and SR01), and two from the Indian Ocean (I06 and I08S). Silicate concentrations for each hydrographic section were first evaluated by collecting and averaging all data within the density range of a respective water mass. Subsequently, water-mass based silicate concentrations from all seven WOCE sections were compiled and averaged for each water mass. There were no major differences among different sections. All of the analyses were performed within the SO poleward of 45^{o}S.

To evaluate the iron concentrations for each water mass the database of Tagliabue et al. (2012, hereafter T12) was co-located with the density structures from the WOCE hydrography. Iron concentrations from the T12 dataset are defined at a specific longitude,

latitude, and depth. Potential density at each location of the iron sample was evaluated using the nearest WOCE station to assign the T12 data points onto water masses with a specific density range. These isopycnal iron concentrations were then averaged to estimate the representative Fe concentrations for each water mass in each ocean basin as well as for each global water mass (Table 1).

Table 1. Water Mass Nutrient Concentrations. The average dissolved iron and silicate concentrations for five major water masses: Subantarctic Mode Water (SAMW), Antarctic Intermediate Water (AAIW), Upper Circumpolar Deep Water (UCDW), North Atlantic Deep Water (NADW), and Antarctic Bottom Water (AABW). Water masses are split by the density ranges given by Sallee et al. (2013).

Water Masses	Iron [mol/m^3]	Silicate [mol/m^3]	Density range [kg/m^3]
SAMW	1.7×10^{-7}	0.01	26.5 – 27
AAIW	2.4×10^{-7}	0.025	27 – 27.5
UCDW	3.4×10^{-7}	0.06	27.5 – 28
NADW	4.0×10^{-7}	0.1	28 – 28.2
AABW	5.9×10^{-7}	0.13	< 28.2

2.2 Box Model

We considered a highly idealized box model to evaluate the coupled cycling of iron (Fe) and silicon (Si) in the Southern Ocean to illustrate the coupled Fe and Si budget in the SO. The water column is vertically divided into a deep box (box 1) and surface box (box 2) as depicted in Figure 2. Overturning circulation, Ψ, brings the nutrient-rich deep water from northern basins into the deep SO where it rises to the surface and returns northward (Figure 2, black arrow). Iron falls out of the water column bound to biogenic silica in diatoms (Figure 2, green dashed arrow). A set of equations below describes the mass balance of Si and Fe.

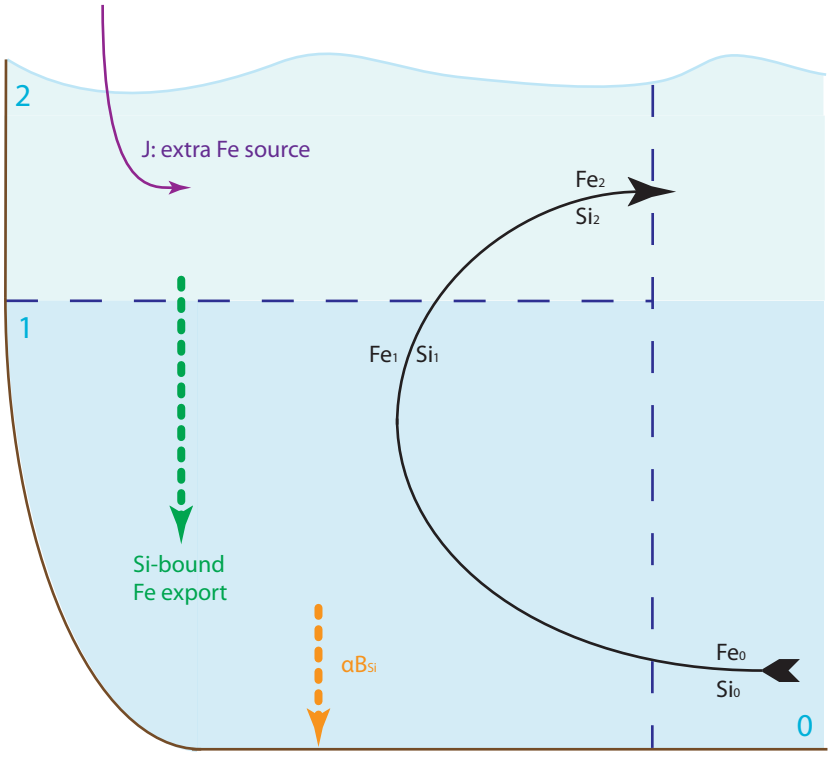

Figure 2. Southern Ocean Nutrient Cycling. An illustration of nutrient cycling in the Southern Ocean. The black arrow indicates the upwelling of deep water to the surface (box 2). The green dashed line indicates biological export of silica bound iron and the purple arrow, J, represents additional sources of iron. The orange dashed line represents the fraction of biogenic silica that is buried in the sea floor.

$$V_1 \frac{\partial Si_1}{\partial t} = \Psi Si_0 - \Psi Si_1 + (1-\alpha) B_{Si} \tag{1}$$

$$V_1 \frac{\partial Fe_1}{\partial t} = \Psi Fe_0 - \Psi Fe_1 + (1-\alpha) B_{Si} R_{bio} \tag{2}$$

$$V_2 \frac{\partial Si_2}{\partial t} = \Psi Si_1 - \Psi Si_2 - B_{Si} \tag{3}$$

$$V_2 \frac{\partial Fe_2}{\partial t} = \Psi Fe_1 - \Psi Fe_2 + B_{Si} R_{bio} + J \tag{4}$$

V_1 and V_2 represent the volume of each box. Nutrient fluxes due to ocean transport are calculated as the product of upwind concentrations and the volume transport

(Ψ). The J term represents the net source of surface iron input including the effects of atmospheric deposition, continental shelves, glacier melt, and other sources excluding precipitation and scavenging losses. A diatom export term, B_{Si}, measured in the units of silica flux, is exported from the surface to the ocean floor. The majority of the biogenic silica flux dissolves back into the deep water but a small fraction (α) is permanently buried in the sediment. Biogenic iron fluxes are coupled to the silicon fluxes through the Fe:Si stoichiometric ratio (R_{bio}), neglecting iron uptake and export by non-diatoms. The range of values for R_{bio} are taken from Ingall et al. (2013). In this study coastal Antarctic diatoms from ice and surface waters were examined untreated and treated with either a trace metal grade 6N hydrochloric acid (HCl) or trace metal grade 30% hydrogen peroxide (H_2O_2) to constrain an iron to silicon ratio (Figure 3). The median Fe:Si ratios of biogenic silica that were untreated, treated with H_2O_2, and treated with HCl were 1.278, 0.458, and 0.045 mmolFe $molSi^{-1}$, respectively. The low estimate from the HCl treated sample fell within a previously published Fe:Si ratio from 0.016 to 0.05 mmolFe $molSi^{-1}$ (Ellwood and Hunter 2000).

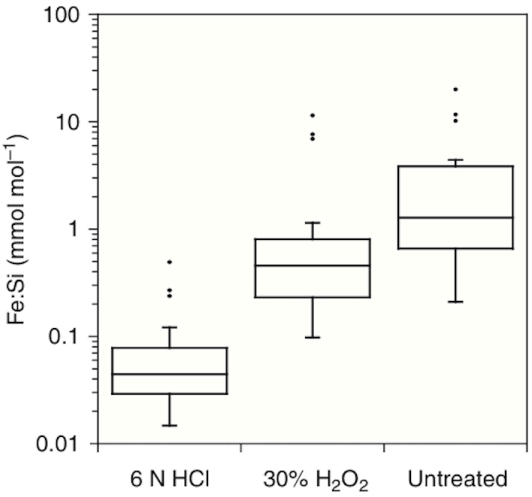

Figure 3. Diatom Iron to Silicon Ratios. Observed Fe:Si ratios of diatom samples from the surface waters and ice in the coastal Antarctic (Ingall et al., 2013). Median Fe:Si ratios (horizontal lines) of biogenic silica that were untreated, treated with H_2O_2, and treated with HCl are 1.278, 0.458 and 0.045 mmol mol^{-1}, respectively. Middle quartiles of each sample group are defined by the boxes. The median across all groups was 0.328 mmol mol^{-1}. Whiskers represent the sample range excluding outliers. Outliers are at least 1.5 times greater or less than the upper or lower quartile. Sample sizes of the untreated, peroxide treated, and acid-washed specimens are 17, 26, and 23, respectively.

2.3 Three-dimensional Ocean Ecosystem and Biogeochemistry Model

To evaluate different Fe:Si diatom ratios in the three-dimensional ocean context, we used an ocean biogeochemistry and ecosystem model based on the MITgcm in offline mode (Marshall et al. 1997), using the circulation fields from Estimating the Circulation and Climate of the Oceans (hereafter, ECCO) product version 3 (Wunsch and Heimbach 2007). This model is a z-coordinate, hydrostatic primitive equation model on a longitude-latitude grid at a resolution of 1 degree by 1 degree and 23 vertical levels with varying thicknesses from 10m near the surface to 250m near the bottom. The circulation fields were previously computed, allowing us to concentrate computational resources on simulating biogeochemical tracers. The ECCO circulation field (1993-2007) is averaged

to form monthly mean climatology, which is then used to transport biogeochemical tracers. A functional-group based ecosystem model (Dutkiewicz et al. 2005) was used in this study. Briefly, the model consists of three nutrients (P, Fe, Si) and two phytoplankton functional groups representing diatoms and picoplankton. The model also contains one zooplankton class. Primary productivity is calculated based on the availability of nutrients and light using the Monod function. The iron chemistry includes complexiation with an organic ligand, a scavenging sink, and a representation of continental shelf sources. Both free iron and ligand-bound iron are assumed to be bioavailable. The organic ligand concentration is set to a uniform constant of 1nM with a conditional stability constant of $10^8\ \mu M^{-1}$.

Diatom productivity is parameterized including limitation by the availability of silicon, phosphorus, and iron, whereas small-sized picoplankton do not require silicon. Both phytoplankton require phosphorus and iron but at different ratios. The model calculates phytoplankton biomass in the units of phosphorus and stoichiometric ratios are used to calculate the uptake of iron and silicon in relation to phosphorus uptake. Throughout this study we kept the diatom Si:P ratio at 25 molSi/molP and adjustments to the diatom Fe:Si ratio were made through changing its Fe:P ratio. For the baseline simulation, we specified the stoichiometric ratios of each plankton type as follows. Picoplankton Fe:P ratios were kept at the model default of 1.0×10^{-4} molFe/molP and the diatom Fe:Si ratio was set to 1.125×10^{-3} molFe/molP to match the low ratio given by Ingall et al. (2013) of 4.5×10^{-5} molFe/molSi (Table 1). The model was spun up for 500 years to reach a quasi-steady state with climatological circulation fields. We will compare the resulting nutrient distributions with observational data in section 3.2.

In order to evaluate nutrient and productivity changes in the global ocean given a higher Fe:Si diatom ratio we then changed the model to match the high ratio given by Ingall et al. (2013) of 1.278 $x10^{-3}$ molFe/molSi (Table 1). This high diatom Fe:Si ratio was implemented by increasing the diatom Fe:P ratio within the model from the baseline 1.125 $x10^{-3}$ to 3.195 $x10^{-2}$ molFe/molP given the Si:P ratio in diatoms of 25 molSi/molP.

CHAPTER 3

RESULTS

3.1 Sensitivity of Iron Demand to Circulation and Diatom Fe:Si Ratio

Here we examine the inferences from the combination of our simple box model and the observed distributions of silicon and iron in the Southern Ocean. The sum of the surface and deep box describes the regional budget where the burial loss of silicon must be balanced by the circulation input in order to maintain a steady state. Using the silicon concentration of the water masses, we first estimate the burial loss of silicon given a range of the upwelling rate.

$$(Si\,burial) = \Psi \Delta Si$$

The burial rate is determined by the product of the overturning volume flux and the silicon concentration difference (ΔSi) between the incoming flux of deep water (set to North Atlantic Deep Water) and the outgoing flux of the upper ocean waters (set to Subantarctic Mode Water). Given the upwelling rate of 8 to 22 Sv (Sallée et al. 2013) and the observed Si distribution, we estimate the burial loss of silicon into the sediment with a magnitude range of approximately 0.75 x10^6 to 2 x10^6 molSi s^{-1}. With a higher upwelling rate, more Si is utilized by phytoplankton and is subsequently buried. Likewise, a larger difference between incoming and outgoing nutrients indicates that more Si is falling out from the surface and buried. Then we calculate the removal of iron from the SO associated with the burial of biogenic silica using the stoichiometric ratio.

$$(Fe\,burial) = R_{bio} \Psi \Delta Si$$

This equation expresses Fe burial in the water column. Similar to Si burial, Fe burial depends on the rate of upwelling and the difference between incoming and outgoing concentrations. The diatom Fe:Si ratio (R_{bio}) is applied to convert Si loss into Fe loss. The associated loss of iron is 33.8 to 2.56x10^3 molFe s^{-1}. This diatom Fe:Si ratio (R_{bio}) can then be contrasted against the Fe:Si ratio of water masses entering and existing the region via meridional overturning circulation (R_{MOC}).

$$R_{MOC} = \frac{\Delta Fe}{\Delta Si}$$

Using the Fe and Si water mass concentrations from Table 1, we calculate a water mass Fe:Si ratio within the water column with a range from 0.0014 to 0.0036 mmolFe/molSi. The difference between R_{bio} and R_{MOC} measures the decoupling between the circulation supply and the burial loss of iron relative to silicon. Recall that the diatom Fe:Si ratio (R_{bio}) range is 0.045 to 1.278 mmolFe/molSi. These observations indicate that R_{MOC} is significantly smaller than R_{bio}, suggesting that deep upwelling of Fe is itself insufficient to balance the burial loss. The non-zero difference between R_{bio} and R_{MOC} indicates that there must be other sources of iron to maintain a steady state. Given the observed R_{bio}, R_{MOC}, and the circulation rates, we can estimate the "missing" source of iron, J (molFe s^{-1}), into the SO in order to close the coupled Fe and Si budget.

$$\begin{aligned} J &= R_{bio}\Psi\Delta Si - \Psi\Delta Fe \\ &= \Psi\Delta Si(R_{bio} - R_{MOC}) \end{aligned}$$

We can easily recognize the simple relationship between J, R_{bio}, and R_{MOC}. When the biogenic ratio is higher than the MOC ratio a larger additional source, J, is required to balance the iron demand from diatom productivity and subsequent burial losses. The high range of uncertainty associated with almost every variable used in the calculation of the

'missing' source, J, produces a wide range of values from 30 to 2.525x10^{3} molFe s^{-1} (Figure 4). Figure 4 shows that the J source will increase with a higher upwelling rate as well as with a higher diatom Fe:Si ratio. The contour angles show that the upwelling rate has a bigger influence on the source magnitude than the ratio size.

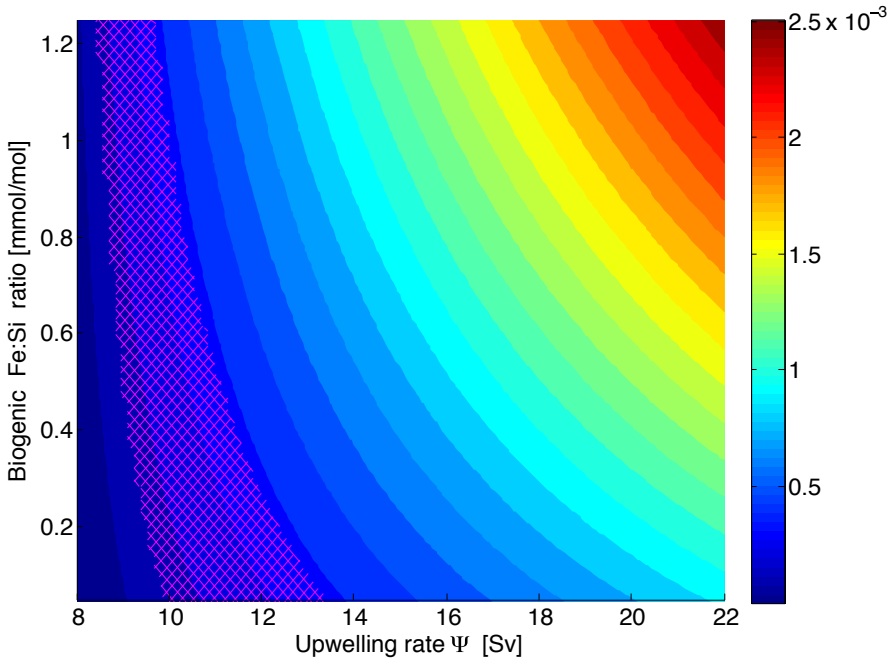

Figure 4. Non-upwelling Sources of Iron. The magnitude of non-upwelling sources of iron, J (MmolFe sec^{-1}), given the upwelling rate and the diatom Fe:Si ratio. The area cross-hatched in magenta indicates a range of J given by Tagliabue et al. (2010) including the sum of observed atmospheric dust, shelf sediment, and iceberg Fe sources.

3.2 3D Model: Baseline Simulation Results

First we evaluate the results from the 500-year long spin-up control run (baseline simulation) as described in section 2.3. The baseline maps capture large-scale patterns of surface nutrient and plankton distributions reasonably well (Figure 5). The modeled phosphate baseline map (Figure 5A) captures the increased phosphate concentrations in

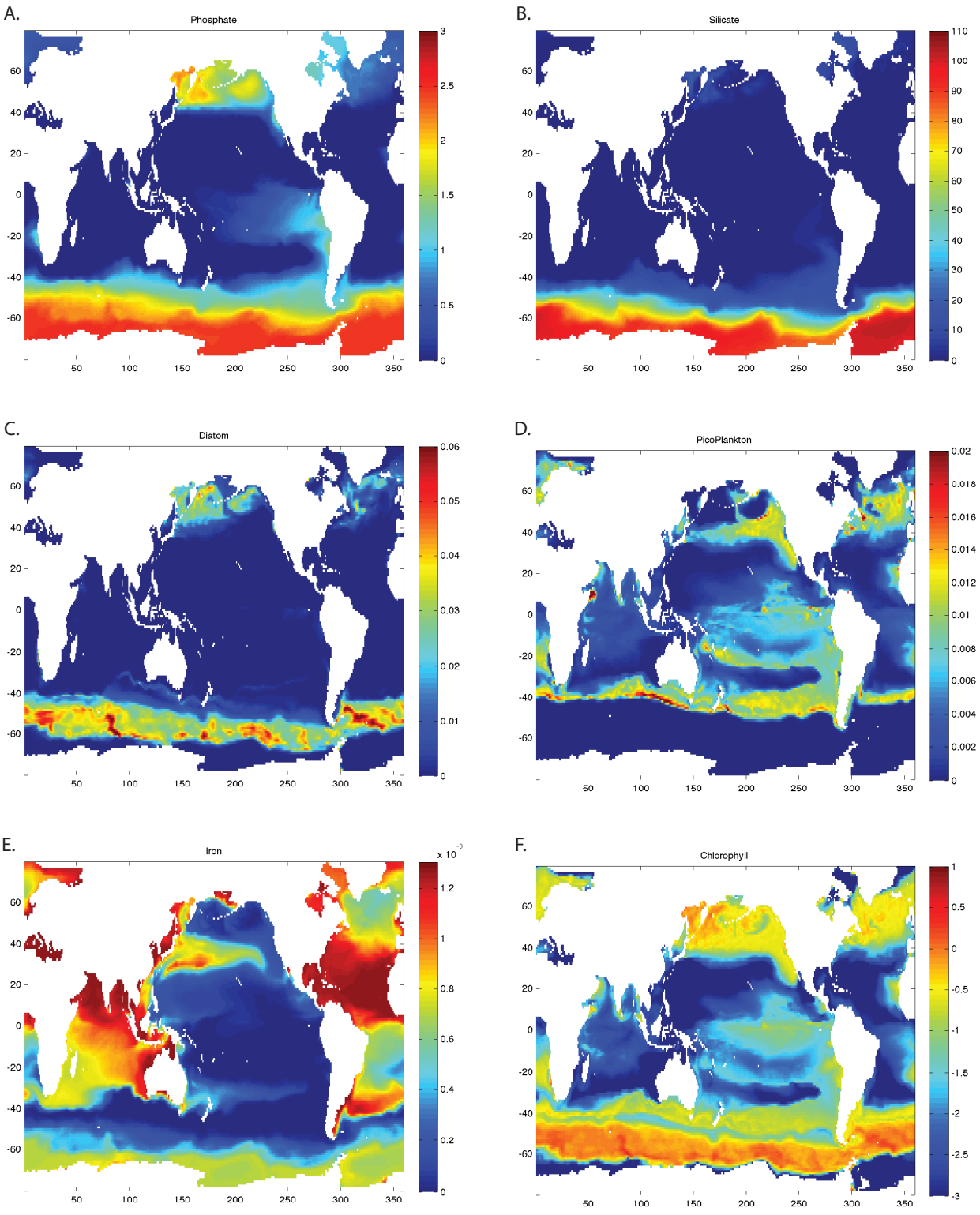

Figure 5. Surface Baseline Model Maps. Surface plots of phosphate (A), silicate (B), diatom (C), picoplankton (D), iron (E), and chlorophyll (F) concentrations from the model baseline 500 year run. Phosphate, silicate, and iron concentrations are in units of mM. Diatom and picoplankton concentrations are in units of mM phosphate. Concentrations of chlorophyll are displayed in log 10 scale and units are mgChl m^{-3}.

the High Nutrient Low Chlorophyll (HNLC) regions such as the Southern Ocean and the Northern Pacific. Silicon concentrations (Figure 5B) are also consistent with observations showing high Southern Ocean concentrations spreading northward. The baseline diatom map (Figure 5C) shows heavy diatom concentrations in high latitude regions especially in the SO. Diatoms tend to dominate high nutrient upwelling regions while the smaller picoplankton tend to dominate the nutrient-depleted oligotrophic gyres (Figure 5C and 5D). Iron concentrations are moderate in the Southern Ocean yet the highest concentrations are seen in regions with elevated dust deposition such as west of Saharan Africa and in the northern Indian Ocean (Figure 5E). The chlorophyll map (Figure 5F) picks up on the diatom and picoplankton hot-spots in the Antarctic and Subantarctic, the northern Pacific and Atlantic, and along the continental coasts in the tropics. In the southern hemisphere, chlorophyll concentrations are highest in and around the areas dominated by the two phytoplankton groups (above and below 40^{o}S).

Direct comparisons between the model and observations are provided in Figure 6 and 7. Meriodional sections of Phosphate and Silicate from the Pacific and Atlantic Oceans are supplied with corresponding cross-sections from the World Ocean Atlas 2009 (Garcia et al., 2010). Clearly the pattern and magnitude of nutrient concentrations are similar between the model and observations. For example, high phosphate concentrations in the South Atlantic are similar in magnitude (2.5 μmol/kg) between the model and observation as well as similar in the extent of northward transport of Antarctic Intermediate Water (to 20^{o}N). Both phosphate and silicate cross-sections do a good job showing the phosphate and silicate traps in the Atlantic sections (Figure 6B and 6D). In general, phosphate is slightly overestimated by the model in the high concentration

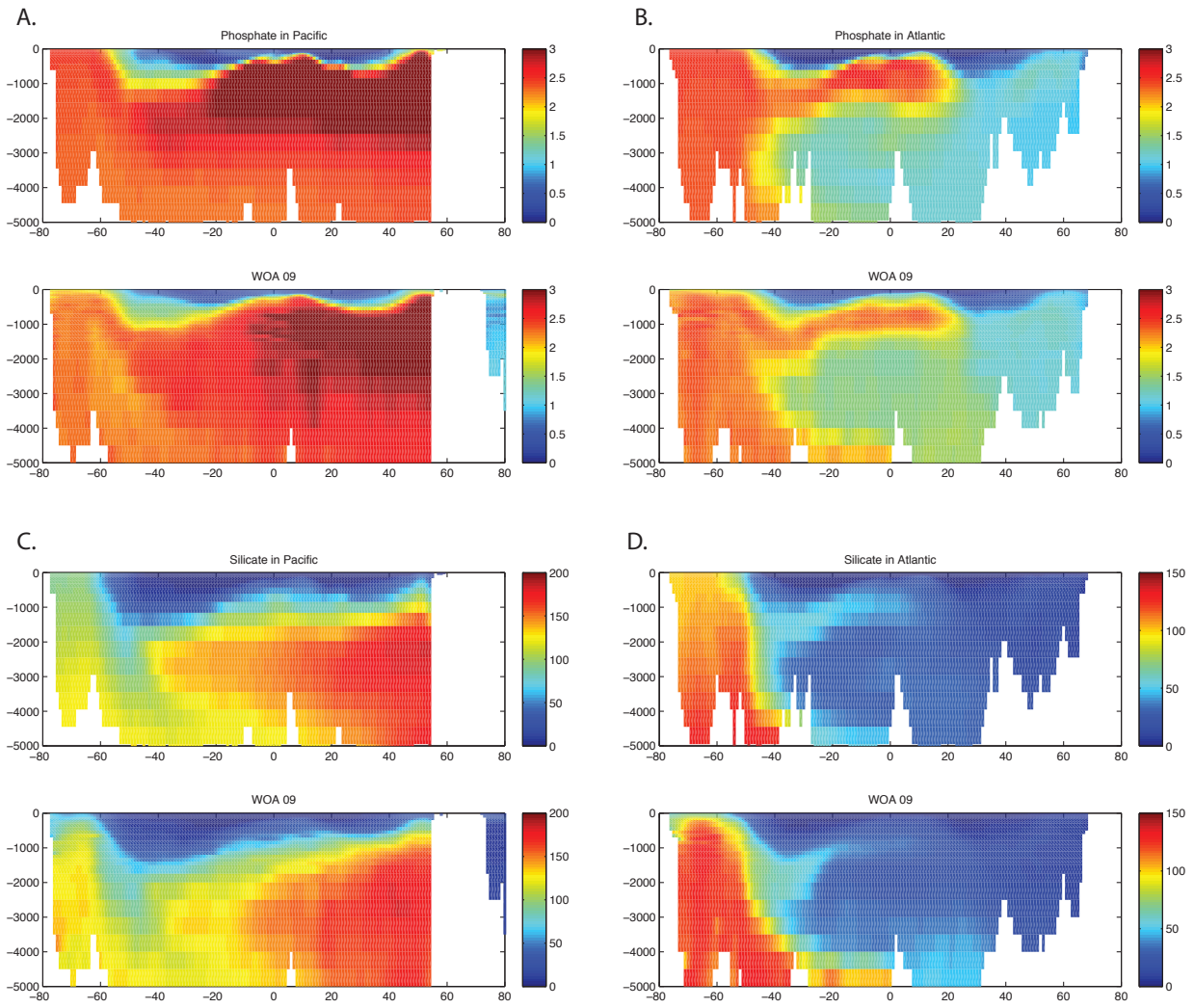

Figure 6. Cross-section Baseline Comparisons with Observation. Meridional sections of phosphate in the Pacific (A) and the Atlantic (B) as well as sections of silicate in the Pacific (C) and the Atlantic (D). The top half of each figure is from the model baseline 500 year control run. The lower half of each figure is observational data from World Ocean Atlas (WOA). Modeled pacific sections were taken from 160^{o}W and modeled Atlantic sections were taken from 30^{o}W. WOA sections were taken from the sites nearest to the 160^{o}W and 30^{o}W lines and concentrations are in units of μM.

regions and silicate is slightly underestimated by the model in the Southern Ocean.

Modeled baseline surface chlorophyll concentrations are compared to SeaWiFS observations in Figure 7. The model slightly underestimates chlorophyll in the tropics and subtropics but captures the high chlorophyll northern Pacific and northern Atlantic. There is little observational chlorophyll data for the SO but our model predicts similar levels of chlorophyll here as in other high nutrient regions. Figure 8 provides meridional sections of iron in the Atlantic and the Pacific. Iron concentrations are low throughout the water column in the low latitudes though concentrations are slightly higher in the Southern Ocean and in very deep water (below 4000m). In the northern Atlantic, iron concentrations are very high within the water column while the northern Pacific shows high concentrations just below the surface. Surface concentrations of iron in general are extremely low in the Pacific cross-section but dust inputs are visible on the surface in the Atlantic section. These plots will be discussed more in the next chapter.

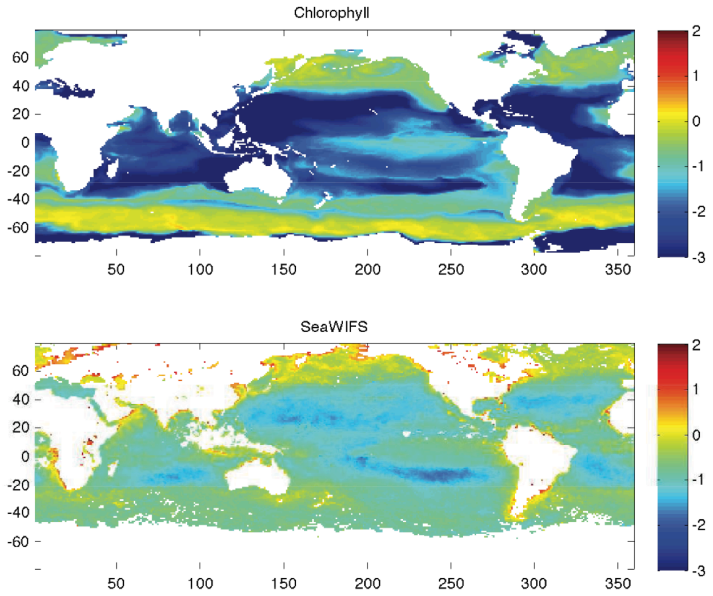

Figure 7. Surface Chlorophyll Baseline Comparison with Observation. The upper surface plot shows chlorophyll concentrations from the model baseline 500 year control run. The lower surface plot is observational data taken from SeaWIFS. Concentrations of chlorophyll are displayed in log 10 scale and units are mgChl m^{-3}.

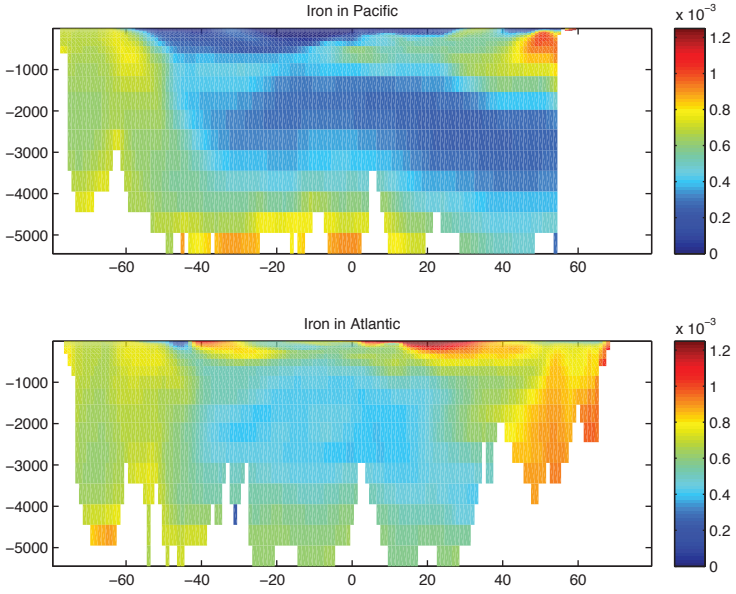

Figure 8. Baseline Iron Cross-section. Meridional section of iron in the Pacific and Atlantic from the model baseline 500 year control run. Modeled pacific sections were taken from 160°W and modeled Atlantic sections were taken from 30°W. Concentrations are in units of μM.

3.3 Sensitivity Experiment Results

After implementing the higher diatom Fe:Si ratio, we see an enormous difference in the concentrations of nutrients and phytoplankton throughout the global ocean. Phosphate and silicate (Figure 9A and 9B) both increase heavily in all regions north of the Southern Ocean. Phosphate increased up to 1.2 μM in the Pacific and silicate increased approximately 80 μM throughout the surface ocean north of the SO (Figure 10A and 10B). Both phosphate and silicate decreased slightly in the Southern Ocean (~0.4 μM and ~20 μM, respectively).

Diatoms decreased in the Southern Ocean (as well as the northern Pacific) by about 0.04 μMP and increased very slightly along the coast of Africa by about 0.02 μMP (Figure 9C). There were also slight increases in diatom activity in the coastal Indian Ocean and around Japan. Picoplankton increased by approximately 0.03 μMP in the subantarctic along 40^{o}S and increased by 0.01 to 0.02 μMP in the mid latitudes throughout the ocean (Figure 9D).

Iron concentrations showed no change in the majority of the Pacific Ocean and decreased by approximately 1 nM in the surface of the Indian and Atlantic Ocean (Figure 9E). Iron also increased slightly around coastal Antarctica by about 0.1 nM with slight decreases (0.5 nM) just north of the coast in the SO. Despite general decreases in surface iron, a large increase in iron concentrations is seen in the subsurface tropical Atlantic (Figure 10C). Chlorophyll represented the changes in phytoplankton activity showing a decrease of about 1 mgChl m^{-3} in the Southern Ocean and an increase of about 1 mgChl m^{-3} in the mid latitudes (Figure 9F). Chlorophyll also decreased slightly in the northern Pacific and Atlantic.

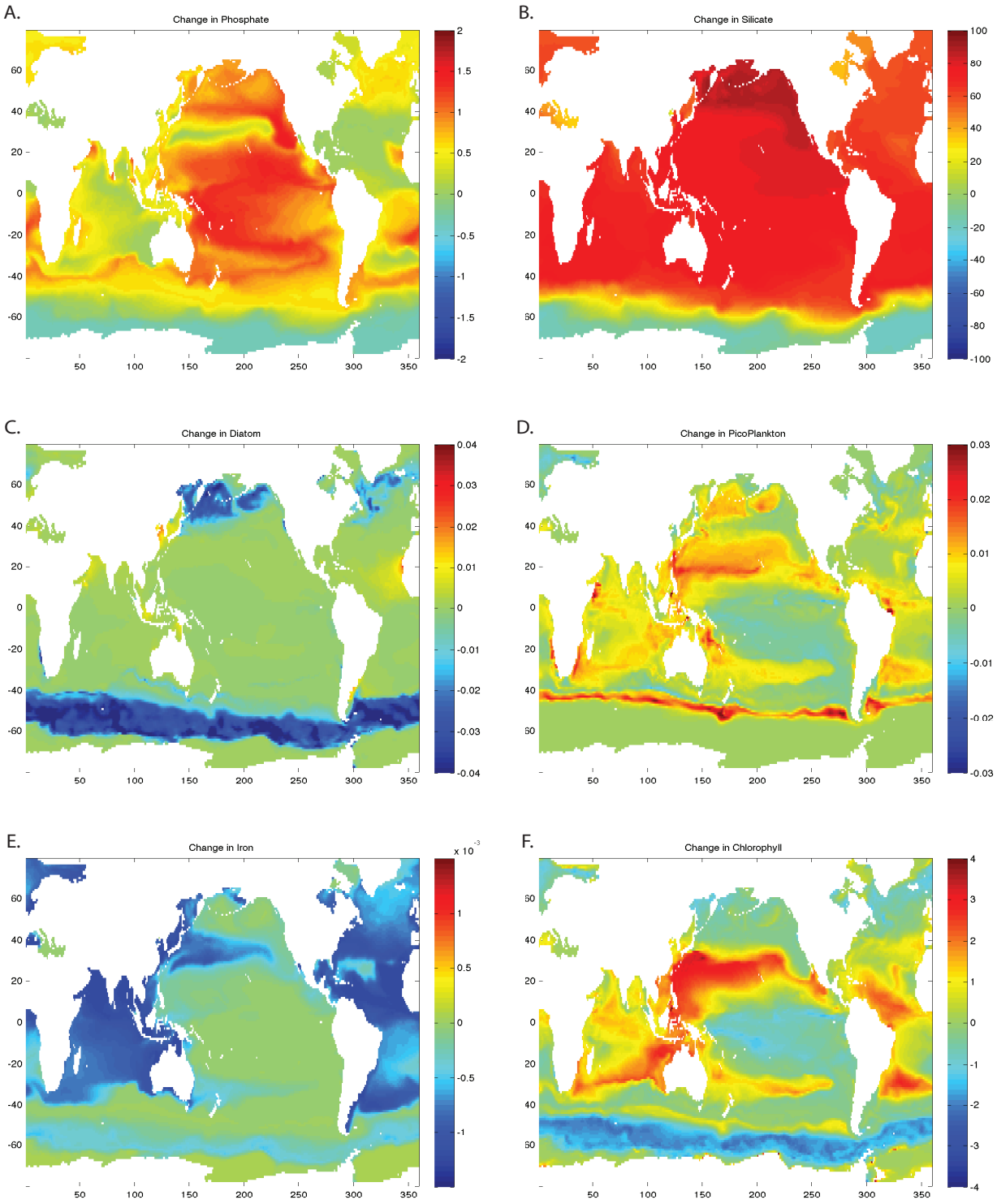

Figure 9. Surface Changes Under a High Fe:Si Ratio. Plots of the changes in phosphate (A), silicate (B), diatom (C), picoplankton (D), iron (E), and chlorophyll (F) concentrations between the simulation with the higher diatom Fe:Si ratio and the baseline simulation (high ratio – low ratio). Phosphate, silicate, and iron concentrations are in units of mM. Diatom and picoplankton concentrations are in units of mM phosphate. Concentrations of chlorophyll are displayed in log 10 scale and units are mgChl m^{-3}.

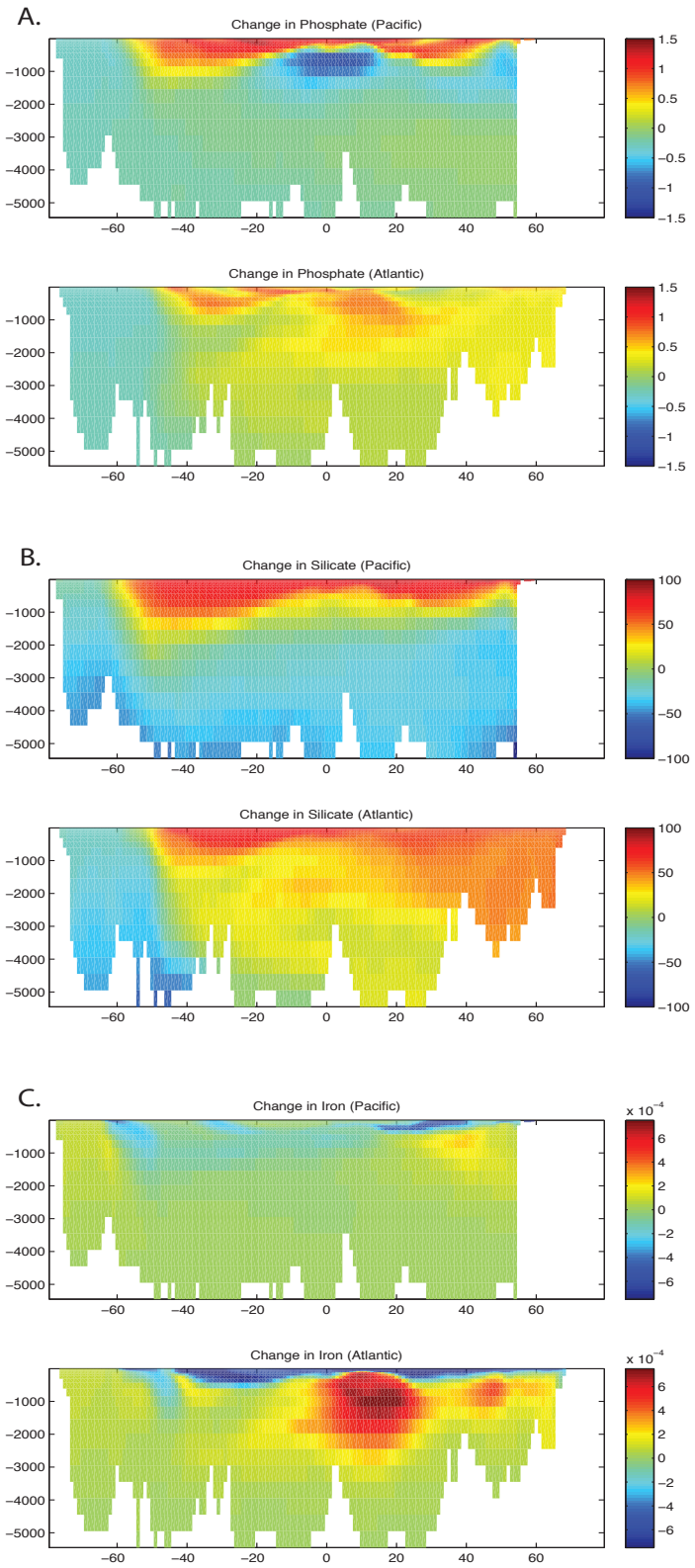

Figure 10. Cross-section Changes Under a High Fe:Si Ratio. Meridional sections of phosphate in the Pacific and the Atlantic (A), sections of silicate in the Pacific and the Atlantic (B), and sections of iron in the Pacific and the Atlantic (C). Modeled pacific sections were taken from 160°W and modeled Atlantic sections were taken from 30°W. Concentrations are in units of μM.

CHAPTER 4

DISCUSSION AND CONCLUSION

The box model calculations show that our computed water mass Fe:Si ratio is much smaller than the observed diatom Fe:Si ratio. Interestingly, the higher diatom ratio at 1.278 mmolFe/molSi reflects untreated samples that potentially provide a more accurate result than the lower acid washed samples (Ingall et al. 2013). Our water mass ratio is an order of magnitude smaller than even the lowest observed diatom ratio. This discrepancy suggests that every mol of diatom export tends to deplete iron in the surface SO relative to silicon. Thus, the upwelling of deep water cannot satisfy the iron demand due to the iron deficit in upwelling water relative to diatom export. This implies that there must either be some large additional source of iron entering the surface SO or some unknown method of silicon removal.

Our calculated range for non-upwelling sources of iron, ~30 to 2525 molFe sec^{-1}, encompasses the range for extraneous sources of iron given by (Tagliabue et al. 2010). In his study, combined sediment, dust, and iceberg iron sources where found to provide ~149 to 379 molFe sec^{-1} (Figure 4, magenta crosshatch). These values fall within the lower range of our estimate. Our calculated value for J could perhaps be a conservative approximation, given that it is based on silicon-utilizing diatoms only and does not consider other non-silicon utilizing phytoplankton. However, biogenic iron associated with non-siliceous cell structures is likely to be remineralized faster than structurally incorporated iron (Ingall et al. 2013). It is important to note that sizable levels of other phytoplankton also thrive in the SO (ex. phaeocystis), however, there are considerably

less studies devoted to the iron requirement of these non-diatom species and thus these plankton are not included in this model.

The complexity and variability of water flow and nutrient movement allow for skepticism regarding models concerning the large and diverse area within the SO. Our box model uses a highly simplified overturning circulation scheme that considers only one SO deep water supply (in the form of NADW) and one surface output (SAMW). In reality, the flow of water into and out of the SO is much more intricate, yet we rely on the two major water masses in our model. With this model set-up, we may overlook additional sources of iron that enter the SO through other upwelling pathways. This simplified water flow, in addition to the wide range of values given for everything from upwelling rate to phytoplankton nutrient ratios, provides a large range for every value that this model tries to constrain. These large areas of uncertainty could be more easily understood with better sampling and information about nutrient concentrations and interactions within the phytoplankton of the Southern Ocean. Understanding these interactions is critical at a global level since the availability of iron can affect not only phytoplankton growth and primary production but also community composition (Moore et al. 2001, Twining et al. 2004). Larger Southern Ocean diatoms require higher iron concentrations in comparison to smaller phytoplankton species (Strzepek et al. 2011) and changes in iron concentration levels could shift microbial populations towards taxa with lower iron requirements (Ingall et al. 2013). Thus, changes in iron availability could affect the magnitude of the carbon export flux (Moore et al. 2001, Twining et al. 2004).

We used an ocean circulation model to look at how increasing the ratio of Fe:Si in diatoms changes the nutrient concentrations and phytoplankton activity in the world's

oceans. After running the baseline (control) run and a sensitivity experiment with the increased diatom Fe:Si ratio for 500 years each we evaluate the observed changes below.

In the baseline silicate plot (Figure 5B), there is an abundance of silicon in the SO throughout the water column. As silicon is transported to the surface via upwelling in the southern Atlantic, diatoms utilize silicon and subsequently sink back into the water column before the silicon has a chance to escape northward through SAMW. This cycle of silicon upwelling, utilization, and sinking is called the silicon trap because of the difficulty silicon has in escaping the Southern Ocean once it is transported there. After the increase in the diatom Fe:Si ratio, the silicon trap weakens considerably. In the Atlantic cross-section (Figure 10B) we see large increases in surface silicon concentrations with a slight decrease in the Southern Ocean potentially indicating that silicon is being used quickly and exported northward in the surface of the Atlantic. Higher silicon content is also seen in the surface of the Pacific Ocean with a decrease in the silicon being horizontally transported beneath the surface indicating the effects of the weakening silicon trap.

The northward horizontal transport that is seen in silicon is also observed in the phosphate model. With an increased diatom Fe:Si ratio there is a decrease in the phosphate content of the SO and an increase in all other surface concentrations (Figure 10A and 9A). The baseline maps of phosphate (Figure 5A, 6A, and 6B) followed by the increased surface concentrations of phosphate north of the SO after the diatom ratio increase indicate a phosphate trap comparable to the previously discussed silicon trap. With the increased diatom Fe:Si ratio both silicon and phosphate rise within the water column in the Southern Ocean via upwelling and are then free to be transported

northward along the surface. Thus the weakening of these silicon and phosphate traps allow for nutrients to begin accumulating on the surface north of the SO (Figure 10A and 10B).

Baseline plots of iron (Figure 5E and 8) show high iron concentration areas where there is a heavy influx of dust to the surface ocean. With a higher diatom Fe:Si ratio, iron was depleted the most in these high dust areas (Figure 9E). This indicates that iron is being exported much more rapidly from the surface in what were previously high iron concentration regions. Thus with an increased diatom Fe:Si ratio iron is preferentially depleted from the surface ocean. With every addition of iron to the surface, iron is exported rapidly as shown by the slight increases in iron concentrations subsurface in the SO and the heavy iron increases in the subsurface low latitude Atlantic (Figure 10C).

Baseline plots of picoplankton and diatom concentrations show that the plankton species occupy opposite areas in the world ocean. Picoplankton have high concentrations in low latitudes around the equator as well as the eastern northern Pacific and circulating the globe in the subarctic at 40^{o}S (Figure 5D). With the higher diatom Fe:Si ratio, picoplankton concentrations increase around but not at these high concentration areas. Increases in the subarctic are seen just below 40^{o}S (Figure 9D) while slight decreases are seen at the 40^{o}S line. Around the equator, picoplankton concentrations decrease slightly with increases occurring just north and south of this area at 20^{o}N and 20^{o}S. With increased diatom Fe:Si ratios, picoplankton respond by inching their territory outward. This seems to be a result of the increased global surface macro-nutrient concentrations and the decrease in the competing diatom concentrations. Thus ocean conditions that benefit the picoplankton community expand under the higher diatom Fe:Si ratio.

Diatom concentrations, which were previously largest in the high latitudes (Figure 5C), decreased significantly in those areas after the increase in diatom Fe:Si ratios. These decreases are most likely associated with the decrease of the silicon trap (and phosphate trap), which allow more of these vital nutrients to escape diatom domain. This occurs since, with the increases in the diatom Fe:Si ratio, iron carries more weight within the diatom structure. With the same amount of iron circulating into the SO and more iron needed to maintain diatom productivity with a higher Fe:Si ratio, it is no surprise that diatoms are less abundant. The "leftover" macro-nutrients then escape northward to be utilized elsewhere. Chlorophyll concentrations reflect these phytoplankton adjustments showing decreases in the SO diatom domain and increases in the mid latitudes with the expanding picoplankton domain. Thus with the increased diatom Fe:Si ratio, the phytoplankton community domains are redistributed across the surface ocean.

While the ratios used in the model are based on observed ratios in diatoms from the Antarctic coast, we use this ratio for diatoms throughout the global ocean. The Fe:Si ratio of diatoms outside of the SO can certainly differ from the ratios observed in diatoms of the Antarctic region. Thus the extreme changes in nutrient concentrations and phytoplankton community structure seen with the use of our high ratio would not be completely characteristic of the ocean conditions even if the high Fe:Si ratio of diatoms in the SO is accurate. However, we feel that even this slightly exaggerated set-up is useful in understanding the reactions of the ocean system even if we cannot rely on the exact values produced by the model. High Fe:Si ratios in diatoms of the SO would still have an impact on the export of nutrients vertically within the SO and impact the magnitude of horizontal nutrient transport escaping the SO. Though the extraordinary

increases in surface macro-nutrient concentrations may not be as severe given a more intricate diatom ratio model layout, the changes in the silicon and phosphate traps within the SO would still produce similar adjustments to surface nutrient concentrations. While perhaps overstated, the changes in nutrient concentrations and phytoplankton productivity shown by the model still reveal the influence of diatom Fe:Si ratios on the ocean system.

The changes shown in the nutrient and phytoplankton concentrations after the diatom Fe:Si ratio is increased do not represent the conditions of the ocean that we accept based on observation. It is not yet clear whether these changes are mainly caused specifically by the diatoms of the Southern Ocean. While regionally changing the Fe:Si ratio of diatoms is beyond the scope of this thesis, it would be a valuable path for future studies.

Given the observations and models presented in this thesis, we can conclude with a few main points. The upwelling of subsurface waters cannot supply enough iron to balance the loss due to diatom production, which indicates that the closed budget requires a significant additional source of iron to the surface Southern Ocean or an additional method of silicon removal. Diatom production preferentially depletes iron relative to silicon in the Antarctic, potentially contributing to iron limitation in this region. A globally higher Fe:Si ratio in diatoms strongly decreases Southern Ocean productivity. In addition, our results indicate that the iron to silicon stoichiometry of diatoms has a large global impact through the distribution of both micro- and macro-nutrients. As stated above, with limited observations of iron and phytoplankton activity within the SO, it becomes difficult to quantify how changes to the ocean environment would effect nutrient concentrations and plankton communities. Yet slight changes in phytoplankton

nutrient ratios produces a large change in the ecological and biogeochemical ocean structure. It is our hope that these issues will be better understood with future sampling and research of Southern Ocean organisms and processes.

REFERENCES

Alvain, S., C. Moulin, Y. Dandonneau and H. Loisel (2008). "Seasonal distribution and succession of dominant phytoplankton groups in the global ocean: A satellite view." *Global Biogeochemical Cycles* 22(3): GB3001.

Baines, S. B., B. S. Twining, M. A. Brzezinski, D. M. Nelson and N. S. Fisher (2010). "Causes and biogeochemical implications of regional differences in silicification of marine diatoms." *Global Biogeochemical Cycles* 24(4): GB4031.

Boyd, P. W., K. R. Arrigo, R. Strzepek and G. L. van Dijken (2012). "Mapping phytoplankton iron utilization: Insights into Southern Ocean supply mechanisms." *Journal of Geophysical Research: Oceans* 117(C6): C06009.

Boyd, P. W. and M. J. Ellwood (2010). "The biogeochemical cycle of iron in the ocean." *Nature Geosci* 3(10): 675-682.

Dutkiewicz, S., M. J. Follows and P. Parekh (2005). "Interactions of the iron and phosphorus cycles: A three-dimensional model study." *Global Biogeochemical Cycles* 19(1): GB1021.

Ellwood, M. J. and K. A. Hunter (2000). "The incorporation of zinc and iron into the frustule of the marine diatom Thalassiosira pseudonana." *Limnology and Oceanography* 45(7): 1517-1524.

Holzer, M., F. W. Primeau, T. DeVries and R. Matear (2014). "The Southern Ocean silicon trap: Data-constrained estimates of regenerated silicic acid, trapping efficiencies, and global transport paths." *Journal of Geophysical Research: Oceans* 119(1): 313-331.

Ingall, E. D., J. M. Diaz, A. F. Longo, M. Oakes, L. Finney, S. Vogt, B. Lai, P. L. Yager, B. S. Twining and J. A. Brandes (2013). "Role of biogenic silica in the removal of iron from the Antarctic seas." *Nat Commun* 4.

Lancelot, C., E. Hannon, S. Becquevort, C. Veth and H. J. W. De Baar (2000). "Modeling phytoplankton blooms and carbon export production in the Southern Ocean: dominant controls by light and iron in the Atlantic sector in Austral spring 1992." *Deep Sea Research Part I: Oceanographic Research Papers* 47(9): 1621-1662.

Marshall, J., C. Hill, L. Perelman and A. Adcroft (1997). "Hydrostatic, quasi-hydrostatic, and nonhydrostatic ocean modeling." *Journal of Geophysical Research: Oceans* 102(C3): 5733-5752.

Martin, J. H., S. E. Fitzwater and R. M. Gordon (1990). "Iron deficiency limits phytoplankton growth in Antarctic waters." *Global Biogeochemical Cycles* 4(1): 5-12.

Moore, J. K., S. C. Doney, D. M. Glover and I. Y. Fung (2001). "Iron cycling and nutrient-limitation patterns in surface waters of the World Ocean." *Deep Sea Research Part II: Topical Studies in Oceanography* 49(1–3): 463-507.

NASA Ocean Biology (OB.DAAC). Sea-viewing Wide Field-of-view Sensor (SeaWiFS) Ocean Color Data, 2014.0 Reprocessing. NASA OB.DAAC, Greenbelt, MD, USA. doi: 10.5067/ORBVIEW-2/SEAWIFS_OC.2014.0.

Parekh, P., M. J. Follows and E. A. Boyle (2005). "Decoupling of iron and phosphate in the global ocean." *Global Biogeochemical Cycles* 19(2): GB2020.

Redfield, A. C. (1958). "The biological control of chemical factors in the environment." *American Scientist* 46: 205-221.

Sallée, J. B., E. Shuckburgh, N. Bruneau, A. J. S. Meijers, T. J. Bracegirdle, Z. Wang and T. Roy (2013). "Assessment of Southern Ocean water mass circulation and characteristics in CMIP5 models: Historical bias and forcing response." *Journal of Geophysical Research: Oceans* 118(4): 1830-1844.

Speer, K., S. Rintoul and B. Sloyan (2000). "The Diabatic Deacon Cell*." *Journal of Physical Oceanography* 30(12): 3212-3222.

Strzepek, R. F., M. T. Maldonado, K. A. Hunter, R. D. Frew and P. W. Boyd (2011). "Adaptive strategies by Southern Ocean phytoplankton to lessen iron limitation: Uptake of organically complexed iron and reduced cellular iron requirements." *Limnology and Oceanography* 56(6): 1983-2002.

Tagliabue, A., L. Bopp, J.-C. Dutay, A. R. Bowie, F. Chever, P. Jean-Baptiste, E. Bucciarelli, D. Lannuzel, T. Remenyi, G. Sarthou, O. Aumont, M. Gehlen and C. Jeandel (2010). "Hydrothermal contribution to the oceanic dissolved iron inventory." *Nature Geosci* 3(4): 252-256.

Tagliabue, A., T. Mtshali, O. Aumont, A. R. Bowie, M. B. Klunder, A. N. Roychoudhury and S. Swart (2012). "A global compilation of dissolved iron measurements: focus on distributions and processes in the Southern Ocean." *Biogeosciences* 9(6): 2333-2349.

Treguer, P. J. and C. L. De La Rocha (2013). "The world ocean silica cycle." *Ann Rev Mar Sci* 5: 477-501.

Twining, B. S., S. B. Baines and N. S. Fisher (2004). "Element stoichiometries of individual plankton cells collected during the Southern Ocean Iron Experiment (SOFeX)." *Limnology and Oceanography* 49(6): 2115-2128.

Wunsch, C. and P. Heimbach (2007). "Practical global oceanic state estimation." *Physica D: Nonlinear Phenomena* 230(1–2): 197-208.